You, R., Liu, W., Chen, J., Lin, C.-H., Wei, D., and Chen, Q. 2016. "Predicting airflow distribution and contaminant transport in aircraft cabins with a simplified gasper model," *Building Performance Simulation*, 9(6): 699-708.

Predicting airflow distribution and contaminant transport in aircraft cabins with a simplified gasper model

Ruoyu You[1], Wei Liu[2,1], Jun Chen[1], Chao-Hsin Lin[3], Daniel Wei[4], and Qingyan Chen[1,2*]

[1] School of Mechanical Engineering, Purdue University, West Lafayette, IN 47907, USA
[2] Tianjin Key Laboratory of Indoor Air Environmental Quality Control, School of Environmental Science and Engineering, Tianjin University, Tianjin 300072, China
[3] Environmental Control Systems, Boeing Commercial Airplanes, Everett, WA 98203, USA
[4]Boeing Research & Technology, Beijing 100027, China

[*] Phone: (765) 496-7562, Fax: (765) 496-0539, Email: yanchen@purdue.edu

Abstract

This study investigated the air distribution and contaminant transport in aircraft cabins with gaspers on using computational fluid dynamics (CFD). If the detailed gasper geometry were used in the CFD simulations, the grid number would be unacceptably high. To reduce the grid number, this investigation proposed a method for simplifying the gasper geometry. The method was then validated by two sets of experimental data obtained from a cabin mockup and a real aircraft cabin. It was found that for the cabin mockup, the CFD simulation with the simplified gasper model reduced the grid number from 1.58 million to 0.3 million and the computing cost from 2 days to 1 hour without compromising the accuracy. In the five-row economy-class cabin of the MD82 airplane, the CFD simulation with the simplified gasper model was acceptable in predicting the distribution of air velocity, air temperature, and contaminant concentration.

Keywords: Jet flow; Computational fluid dynamics (CFD); Experimental validation; Turbulence modeling; Enclosed environments.

1. Introduction

Over the last few decades, the transmission of airborne infectious diseases such as tuberculosis (Kenyon et al., 1996), influenza (Moser et al., 1979), and severe acute respiratory syndrome (Olsen et al., 2003) has been observed in aircraft cabins. As more and more passengers travel by air (ACI, 2007), they demand a cleaner and healthier cabin environment. Gaspers, the small, circular, and adjustable vents installed in aircraft cabins for each passenger above the seat, are used in commercial airplanes as a personalized ventilation system for regulating thermal comfort. Turing on gaspers may affect the air distribution in an aircraft cabin (You et al., 2016) and further influence contaminant transport. It is crucial to investigate the air distribution and contaminant transport in cabins with gaspers turned on in order to evaluate the usefulness of gaspers in protecting passenger from exposure to contaminants.

Several experimental studies have been conducted in this area. Dai et al. (2015) measured the flow field of a gasper-induced isothermal jet with a high-precision hotwire anemometer. You et al. (2016) used a particle imaging velocimetry (PIV) technique to measure the interactions among the gasper-induced flow, the main flow in the cabin, and the thermal plume from a passenger in a cabin mockup. To study the impact of gaspers in actual airliners, Li et al. (2016) measured the distributions of air velocity, air temperature, and contaminant concentrations in the economy-class cabin of a retired MD-82 airliner with two fifths of the gaspers open and compared them with the distributions when the gaspers were off. They found that turning on the gaspers would not necessarily improve the air quality.

Conducting experiments in a real aircraft cabin is very expensive, but numerical methods have also been employed to investigate the air distribution and contaminant transport in aircraft cabins with gaspers on. Among these methods, computational fluid dynamics (CFD) has been widely used because it is informative and economical (Liu et al., 2012a). For instance, Zhang et al. (2009) used CFD to predict the air distribution and gaseous and particulate contaminant transport in a half-occupied, twin-aisle aircraft cabin mockup. Liu et al. (2013) used experimental data to evaluate the performance of various turbulence models in predicting the air distribution in the first-class cabin of an MD-82 airliner. Gupta et al. (2012) assessed the risk of airborne infection in aircraft cabins by using CFD to predict the spatial and temporal distributions of droplets exhaled by a passenger in a seven-row, twin-aisle aircraft cabin. Although the above studies are interesting, in all of these cases it was assumed that the gaspers were turned off.

To study gasper-induced flow, Shi et al. (2015) used detailed gasper geometry in CFD to predict the air distribution of a jet from a gasper. Describing the geometry required millions

of cells. You et al. (2016) used the detailed geometry of the gasper in predicting the air distribution in half of a one-row, single-aisle cabin mockup with one gasper turned on. They found that the grid around the gasper accounted for 28% of the total grid, while the volume of this region was only 0.0006% of the total cabin mockup volume. If detailed gasper geometry were applied in a section of a cabin (where a minimum of five rows are needed for contaminant transport), the total grid number used to discretize the domain would be at least 20 million. The computation would require a computer cluster with at least 64 GB RAM. However, both of the above studies found that the jet flow from the gasper developed similarly to a round jet, suggesting that the gasper could be simplified as a round nozzle in the CFD simulations.

The literature review indicated that CFD could be an informative tool for studying air distribution and contaminant transport in airplane cabins with gaspers on, but the computing costs would be unacceptably high. This high cost is a result of the large grid number needed to represent the detailed geometry of the gaspers. For affordable CFD simulations, it is essential to reduce the grid number for the gaspers without compromising accuracy. This need forms the objective of the study reported in this paper.

2. Method for Simulating Air Distribution and Contaminant Transport in a Cabin with Gaspers on

The jet behavior observed in previous studies (Dai et al., 2015; You et al., 2016) appears to be similar to that of a round jet. The present investigation explored the possibility of simplifying the gasper geometry as a round nozzle for CFD simulations. A simple round nozzle (simplified gasper) was used to replace the complex gasper for predicting the air distribution and contaminant transport in cabins. The results predicted with the simplified gasper were validated by experimental data from a cabin mockup and a real aircraft cabin.

2.1 Brief introduction of the CFD method used

This investigation used the SST k-ω model (Menter, 1994) for predicting the air distribution in cabins with gaspers on, because it was able to accurately predict the air distribution in the critical area (You et al., 2016). The SST k-ω model is a Reynolds-averaged Navier-Stokes (RANS) model. For an incompressible Newtonian flow, the RANS equation can be written as:

$$\frac{\partial U_i}{\partial t}+\frac{\partial}{\partial x_j}(U_jU_i)=-\frac{1}{\rho}\frac{\partial P}{\partial x_i}+\frac{\partial}{\partial x_j}(\frac{\mu}{\rho}(\frac{\partial U_i}{\partial x_j}+\frac{\partial U_j}{\partial x_i})-\overline{u_iu_j})+S \quad (1)$$

where U is the Reynolds-averaged air velocity, t the time, x the coordinate, ρ the air density, P the pressure, μ the air viscosity, u the fluctuating air velocity, and S the source term. The bar stands for Reynolds average. The SST k-ω model uses the Boussinesq eddy-viscosity approximation to link the turbulence Reynolds stresses to eddy-viscosity:

$$-\overline{u_i u_j} = \frac{\mu_t}{\rho}\left(\frac{\partial U_i}{\partial x_j} + \frac{\partial U_j}{\partial x_i}\right) - \frac{2}{3}\delta_{ij}k \tag{2}$$

where $\overline{u_i u_j}$ is the turbulence Reynolds stress, μ_t the eddy viscosity, and k the turbulence kinetic energy. The k can be expressed as:

$$k = \frac{1}{2}\overline{u_i' u_i'} \tag{3}$$

In the SST k-ω model, the turbulent eddy viscosity is calculated by:

$$\mu_t = \frac{\rho k}{\omega}\frac{1}{\max\left[\frac{1}{\alpha^*}, \frac{SF_2}{a_1\omega}\right]} \tag{4}$$

where α^* is a coefficient that damps the turbulent viscosity, causing a low-Reynolds-number correction; S is the strain rate magnitude; F_2 a blending function; a_1 a constant; and ω the specific dissipation rate.

Thus, the model needs to solve two additional governing equations, one for k and the other for ω. The equation for k is

$$\frac{\partial}{\partial t}(\rho k) + \frac{\partial}{\partial x_i}(\rho k U_i) = \frac{\partial}{\partial x_j}\left[(\mu + \frac{\mu_t}{\sigma_k})\frac{\partial k}{\partial x_j}\right] + G_k - Y_k \tag{5}$$

where σ_k is the turbulent Prandtl number for k, G_k the generation of turbulence kinetic energy due to mean velocity gradients, and Y_k the dissipation of k due to turbulence. This model calculates the ω by:

$$\frac{\partial}{\partial t}(\rho\omega)+\frac{\partial}{\partial x_i}(\rho\omega U_i)=\frac{\partial}{\partial x_j}\left[(\mu+\frac{\mu_t}{\sigma_\omega})\frac{\partial\omega}{\partial x_j}\right]+G_\omega-Y_\omega+D_\omega \quad (6)$$

where σ_ω is the turbulent Prandtl number for ω, G_ω the generation of ω, Y_ω the dissipation of ω due to turbulence, and D_ω the cross-diffusion term. To simulate the buoyancy effect, the Boussinesq approximation was adopted in this study. Note that the SST k-ω model does not consider the production due to buoyancy in the k equation or the ω equation (Menter, 1994).

Contaminant transport was simulated by the Eulerian method (Zhang and Chen, 2007) by:

$$\frac{\partial\phi}{\partial t}+\frac{\partial}{\partial x_i}(\rho\phi U_i)=\frac{\partial}{\partial x_j}\left[\Gamma_\phi\frac{\partial\phi}{\partial x_j}\right]+S_\phi \quad (7)$$

where ϕ is the SF_6 concentration, Γ_ϕ the diffusion coefficient, and S_ϕ the mass flow rate of SF_6 source per unit volume. A detailed description of all the terms in the equations can be found in the ANSYS Fluent manual (ANSYS, 2010).

The SIMPLE algorithm (Patankar, 1980) was used to couple the pressure and velocity. This study used the PRESTO! scheme for pressure discretization and the second-order upwind scheme for discretizing all the other variables. Two convergence criteria were used in this study. First, the scaled residuals for velocity, turbulence, and energy had to reach 10^{-4}, 10^{-4}, and 10^{-6}, respectively. Second, this study monitored the velocity magnitude at distances of 0.1 m, 0.25 m, and 0.5 m from the gasper outlet, and the first decimal number of the velocity magnitude could not change with further iteration after the simulation results had converged.

2.2 Simplification of the gasper for CFD simulations

This study proposed the use of a round jet in place of the jet from the gasper. If the round jet has the same downstream velocity field as that from the gasper, the complex gasper geometry can be simplified as a round nozzle in CFD simulations. This section describes our approach.

In order to obtain the downstream velocity field of the gasper-induced jet, a CFD calculation was first carried out with the detailed gasper geometry as shown in Figure 1(a), placed in a space as shown in Figure 1(b). The dimensions of the space were 0.6 m (L) × 0.6 m (W) × 0.6 m (H), as recommended by Shi et al. (2015) in order to capture the decay in the centerline velocity with distance. The bottom wall was defined as the pressure outlet, and all other walls were defined as no-slip walls. The supply flow rate was 1.2 L/s in this investigation, and the

jet was isothermal.

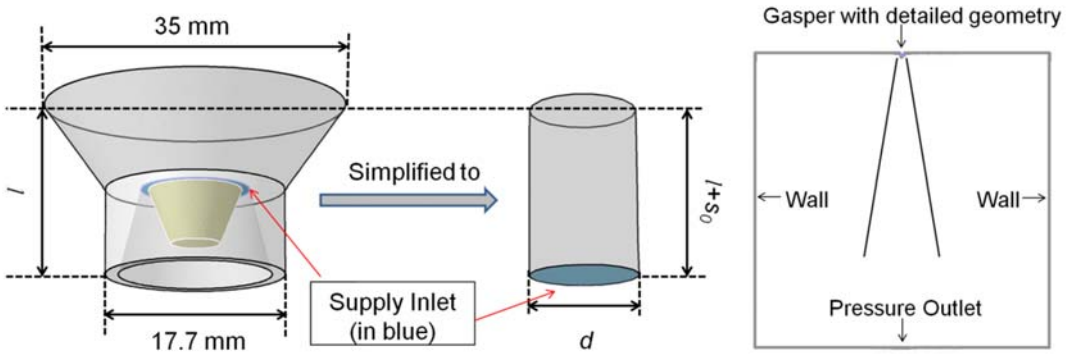

(a) (b)

Figure 1 (a) Comparison of the detailed gasper geometry and the simplified gasper geometry; (b) case setup for studying the jet.

With the use of the CFD method described in the previous section, the centerline velocity (U_m) of the jet was found to decay as a function of axial distance (s) as shown in Figure 2. The axial distance is defined as the distance from the lower edge of the gasper. The centerline velocity decay was then used to determine the dimensions of the round nozzle.

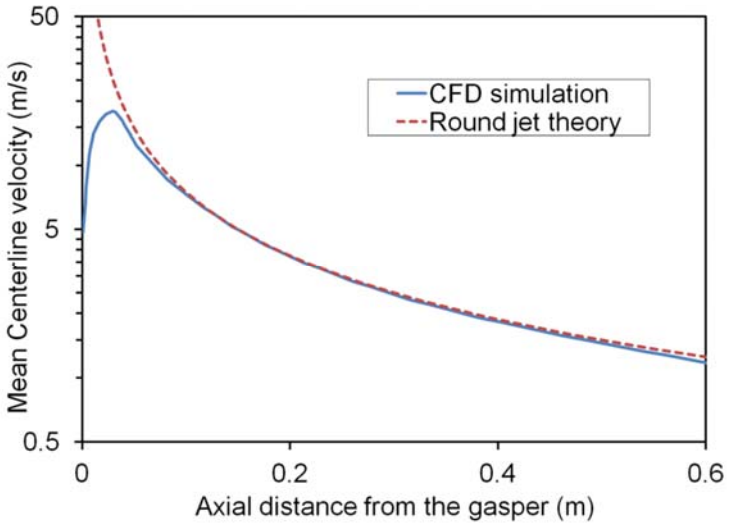

Figure 2 Centerline velocity decay as a function of axial distance for two types of jet.

For the round jet in the developed region, the non-dimensional centerline velocity can be expressed as (Pope 2000):

$$\frac{U_m}{U_{m,0}} = \frac{B}{(s - s_0)/d} \tag{8}$$

where $U_{m,0}$ is the exit velocity of the round jet, B a constant of 6.2 (Hussein et al., 1994), s_0 the position of the virtual jet origin, and d the diameter of the round inlet.

From equation (8), the U_m decay with s could be expressed as:

$$U_m = \frac{B^*}{s - s_0} \tag{9}$$

where B^* is an empirical constant. To ensure that the gasper-induced flow has the same U_m profile as that of the round jet, the values of B^* and s_0 can be determined by least square regression from the predicted U_m profile as shown in Figure 2. In this case, the least square regression in the fully developed jet region led to a B^* of 0.75 and an s_0 of 0 with an R^2 of 0.99. Because the s_0 of the round jet is assumed in theory to be 0, the calculated s_0 can be used to determine the location of the nozzle outlet. The B^* can then be used to determine the diameter of the round nozzle, d, as shown in Figure 1(a).

Combining Eqs. (8) and (9) yields the following expression:

$$B^* = BdU_{m,0} \tag{10}$$

Since the flow rate Q from the round nozzle is

$$Q = \frac{\pi}{4} U_{m,0} d^2 \tag{11}$$

Eqs. (10) and (11) can be solved to yield

$$U_{m,0} = \frac{\pi B^*}{4QB^2} \tag{12}$$

$$d = \frac{4QB}{\pi B^*} \tag{13}$$

so that the diameter and supply air velocity of the nozzle can be determined.

For the gasper shown in Figure 1(a), the B^* is 0.75 and Q is 1.2 L/s. The corresponding d is 12.64 mm, and $U_{m,0}$ is 9.56 m/s. The complex gasper has thus been simplified as a round nozzle for CFD prediction of air distribution in a space with the gasper on. This effort can reduce the grid number required to discretize the gasper because the nozzle is very simple. As a result, the computing cost is decreased without compromising the accuracy of the CFD prediction.

3 Validation of the simplified gasper model for simulating the gasper flow

To validate the claim above in regard to the computing cost and accuracy of the CFD prediction, this study used two cases: a cabin mockup (You et al., 2016) and a real cabin (Li

et al., 2016). In the mockup, high-quality air velocity distribution measurements were performed with PIV. In the real cabin, which was a section of an MD-82 economy-class cabin, the measured distributions of air velocity and airborne contaminant were simulated by use of a tracer gas. The measured data can be used for the validation of air distribution in cabins with the simplified gaspers.

3.1 Cabin mockup case

The cabin mockup was half of a one-row cabin that simulated a Boeing 737 as shown in Figure 3. The main air supply to the cabin flowed downward from a linear diffuser on the ceiling and was exhausted at floor level. A gasper was installed on the inclined surface of the ceiling to provide personalized ventilation to a passenger simulated by a heated box, as shown in the figure. The box was placed in the middle of the cabin with 75 W of sensible heat. The PIV system was used to obtain the flow in the critical area where the main cabin flow, gasper-induced flow, and thermal plume from the human simulator encountered one another, as shown in the area enclosed by the dashed lines in Figure 3. The experiment included the measurement of the surface temperature, inlet air temperature, and flow rates, which were used as boundary conditions for the CFD simulation.

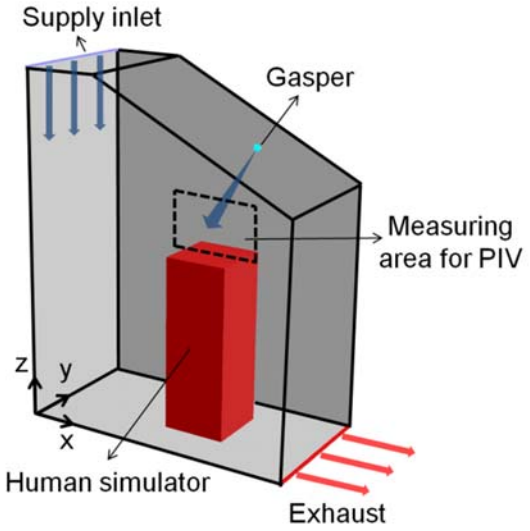

Figure 3 The sketch of the aircraft cabin mockup.

The CFD simulation used the simplified gasper model, in which the diameter d was 12.64 mm and s_0 was 0 as shown in Figure 1(a). This study considered three grid resolutions, 0.2, 0.3, and 0.65 million for CFD grid independence test. The resolution of 0.3 million was found to be sufficient to model the flow in the chamber. Figure 4 compares the distribution of the grid structure near the gasper for different gasper geometry models. The grid size for the

detailed gasper geometry model was much smaller compared to that for the simplified one. As a result, using the complex gasper geometry would increase the total grid number to 1.58 million (You et al., 2016).

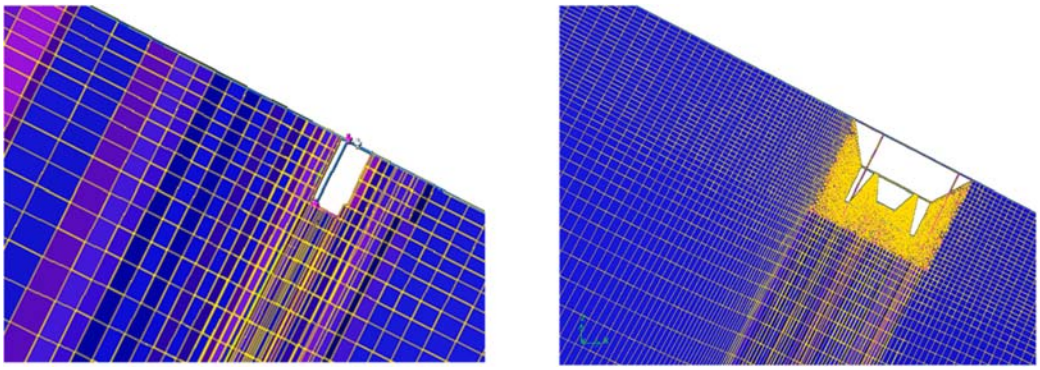

(a) (b)

Figure 4 Comparison of the grid structure near the gasper for (a) the simplified gasper geometry model, and (b) the detailed gasper geometry model.

Figure 5 compares the air velocity distribution predicted by the simulation with the data measured by PIV in the critical area. The results of the CFD simulation with the detailed gasper geometry (You et al., 2016) are also plotted in the figure for comparison. The CFD predictions with the simplified gasper model correctly captured the jet from the upper right section to the lower left section, as well as the circulation at the lower right. Moreover, the jet direction and velocity magnitude predicted by CFD with the simplified gasper model were similar to those predicted with the actual gasper geometry. In summary, the CFD simulation with the simplified gasper model accurately predicted the air distribution in the critical area, and no obvious discrepancy was observed between the air distribution predicted by CFD with the simplified gasper model and that with the actual gasper geometry.

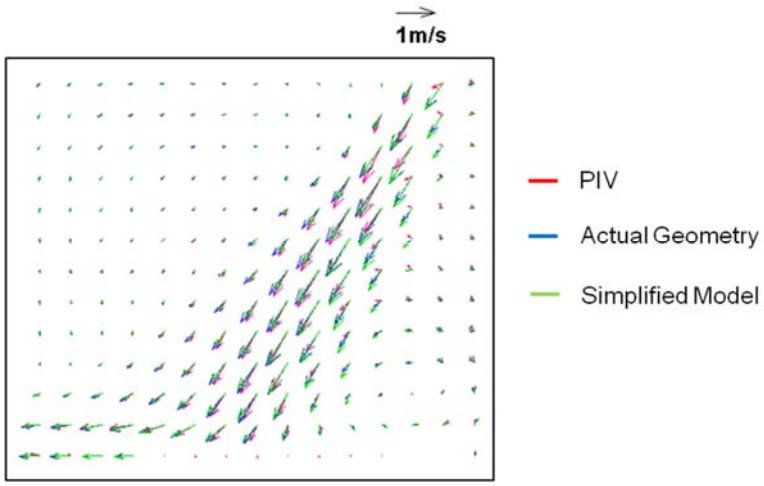

Figure 5 Comparison of the predicted airflow field by CFD with different gasper geometry models and experimental data in the critical area.

For quantitative analysis of the performance of the simplified gasper model, Figure 6 shows the horizontal and vertical velocity profiles at five lines in the critical area predicted by CFD and measured by PIV. In the horizontal velocity profiles shown in Figure 6(a), the results simulated by CFD with the simplified gasper model capture the measured peak velocity, as do the results with the actual gasper geometry. In the vertical velocity profiles shown in Figure 6(b), the CFD results with the simplified gasper model agree reasonably well with the experimental data. When the results predicted by CFD with the two gasper geometry models are compared with the experimental data, it can be seen that the prediction with the simplified gasper model was slightly better for the horizontal velocity and slightly worse for the vertical velocity. The results predicted by the two models are comparable.

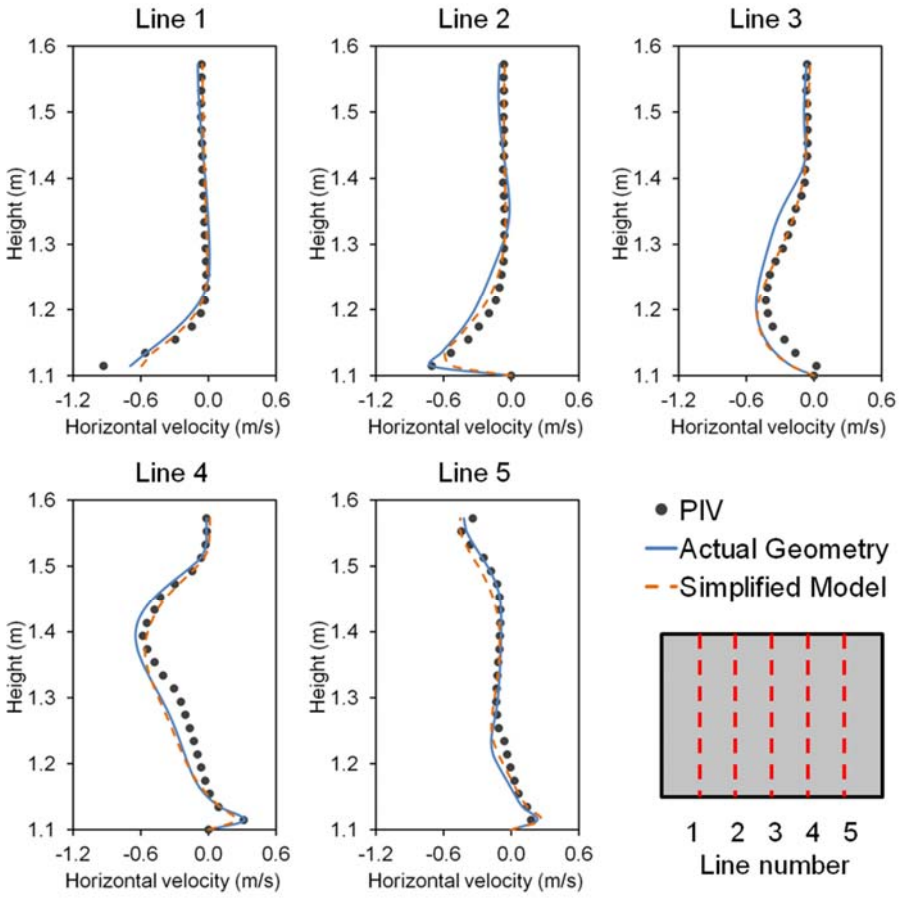

(a)

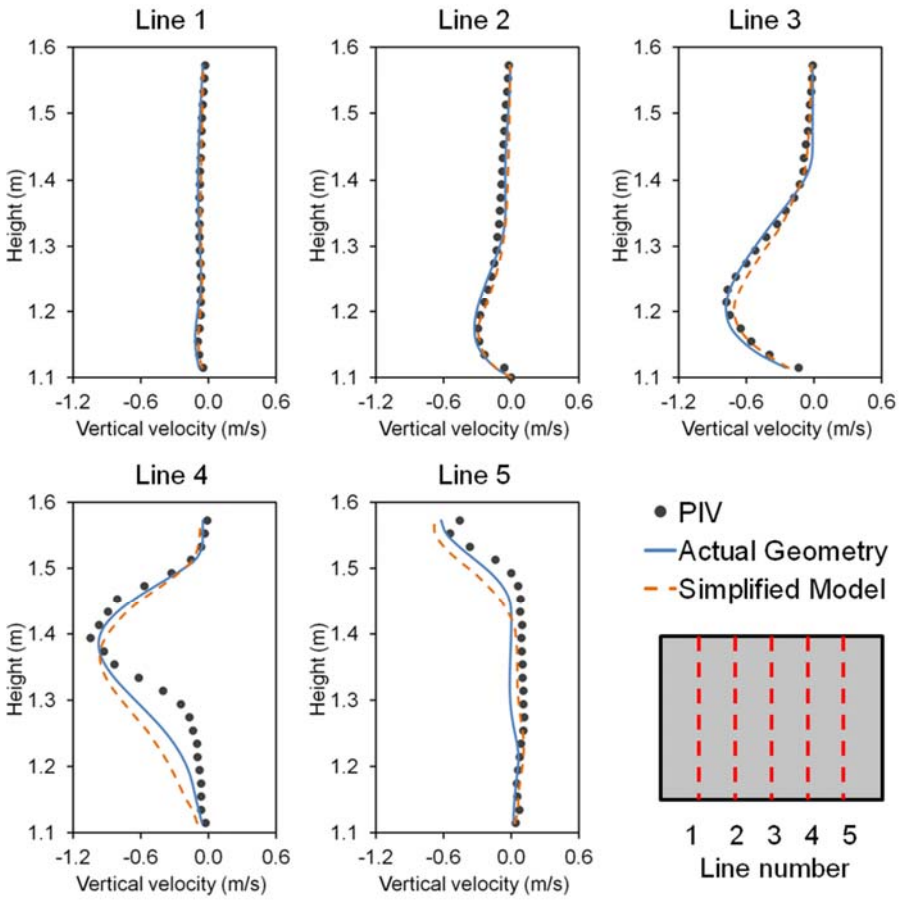

(b)

Figure 6 Comparison of the predicted and measured velocity profiles in the critical area: (a) horizontal velocity and (b) vertical velocity.

On the basis of the analysis above, Table 1 further compares the grid cells used and the computing time required to meet the convergence criteria discussed in Section 2.1. Since the actual gasper geometry was more complicated than that of the simplified gasper model, the grid size needed to depict the gasper details was much smaller. Thus, the total grid number for the case with the actual gasper geometry was more than five times that for the case with the simplified gasper model. In addition, the actual geometry required 17601 iterations to achieve convergence, whereas the simplified geometry required only 4251 iterations. The difference in total grid number and computing cost resulted in a huge difference in computing time between the two cases. This investigation used a workstation with a quad-core processor of 3.0 GHz and RAM of 16 GB. The computing time for the case with the actual gasper geometry was two days, while using the simplified gasper model reduced the computing time to only 1 hour. Moreover, as discussed above, the CFD simulation using the simplified gasper model predicted the air distribution with similar accuracy to that of the simulation using the actual geometry. Thus, the simplified gasper model reduced the total grid number and

computing time needed to predict the air distribution in the cabin mockup without compromising accuracy.

Table 1. Evaluation of the simplified gasper model.

	Actual gasper geometry	Simplified gasper model
Grid number	1.58 million	0.3 million
Computing cost	17601 iterations	4251 iterations
Computing time	2 days	1 hour
Accuracy	Similar	

3.2 Real cabin case

Li et al. (2016) conducted air distribution measurements in a section of the economy-class cabin of an MD-82 plane with the geometric configuration shown in Figure 7(a). Each row of the cabin had five seats and five gaspers. Air was supplied to the cabin as a whole from the diffusers at the cabin shoulders on both sides and was exhausted on both sides near the floor. Heated manikins were placed on the seats to simulate passengers. As shown in Figure 7(b), a gas mixture of 1% SF_6 and 99% N_2 was placed as a contaminant source in aisle seat 9C with an SF_6 mass flow rate of 1.02×10^{-6} kg/s. The gaspers in columns B and C were open during the test. As shown in Figure 7(b), Li et al. (2016) measured the distributions of air temperature, air velocity, and an airborne contaminant simulated by a tracer gas in five cross sections (CS7 to CS11, indicated by solid red lines) and three longitudinal sections (ASLS, CALS, and WSLS, indicated by dashed red lines). The experiment also measured the time-averaged velocity and velocity fluctuation at the diffusers; air temperature and airflow rate for each opened gasper; and the temperature of the cabin walls, ceiling, floor, manikins, and seats.

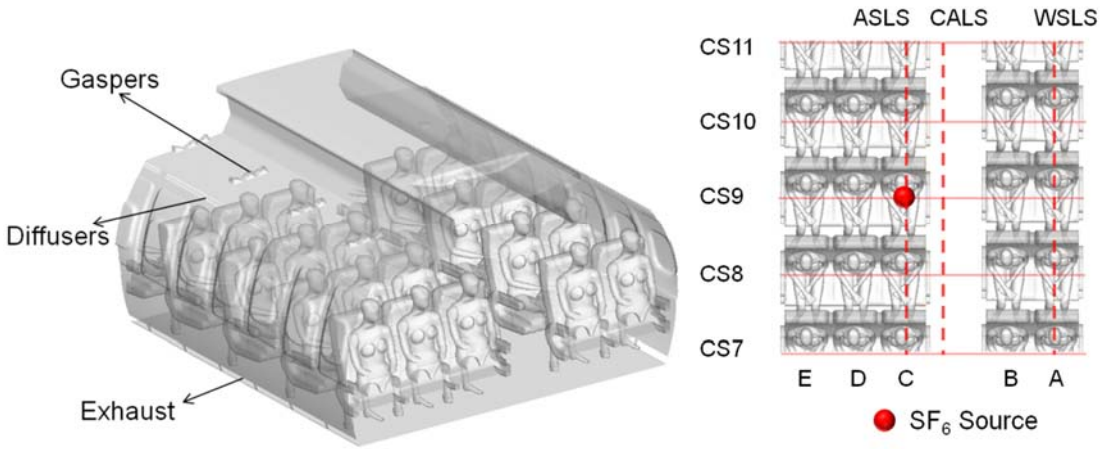

(a) (b)

Figure 7 (a) Sketch of the five-row MD-82 economy-class cabin and (b) measuring positions by Li et al. (2016).

The present investigation simplified the gaspers in the cabin as simple nozzles in the CFD simulation. The gaspers in the economy-class cabin were different from the ones used in the half of the one-row cabin; the diameter of the nozzle was 10.03 mm, and s_0 was 0.0 mm as determined by the method outlined in Section 2.2. The measured air velocity, temperature, and SF6 concentration at the cross sections in the front (CS7) and back (CS9) were used as the boundary conditions in the CFD simulation. Thus, the experimental data at the remaining three cross sections and three longitudinal sections could be used to validate the CFD results. Three grid resolutions, 1.65, 2.98, and 6.37 million, were tested for CFD grid independence, and the resolution of 2.98 million passed the test. The CFD simulation results converged after 8004 iterations. The total computing time was about 1 day on the same computer as that used for the half of the one-row cabin.

This study compared the simulated distributions of the air velocity, air temperature, and contaminant concentration with the measured data in the cabin. Figure 8 shows the comparison in two cross sections (CS8 and CS9) and two longitudinal sections (ASLS and CALS). The circles in Figures 8(a) and (b) represent the arms of the passengers that cut through the cross sections, while the V-shapes below the circles represent the thighs of the passengers on the seats.

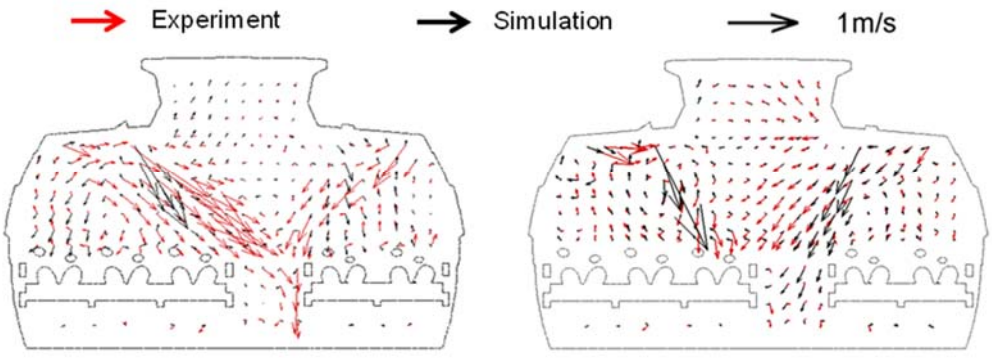

(a) (b)

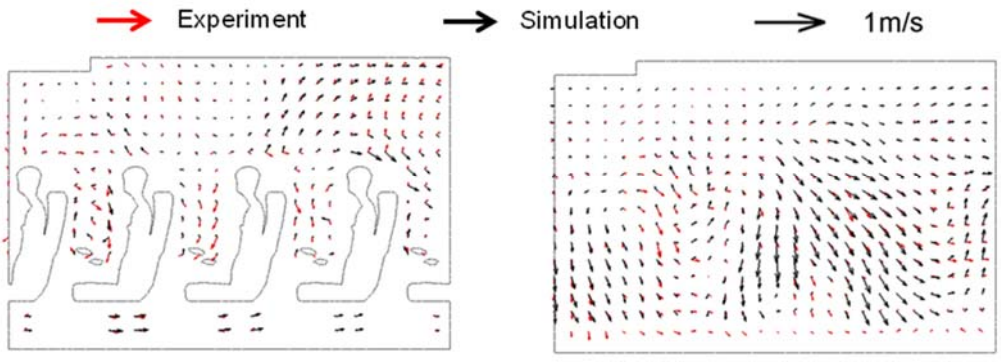

(c) (d)

Figure 8 Comparison between the predicted and measured airflow field in (a) CS8, (b) CS9, (c) ASLS, and (d) CALS.

The experimental data in CS8 shows a strong jet from gasper, while that in CS9 is not obvious. Since the gasper is very small, and the jet velocity gradient is very large, the flow field near the gasper is very sensitive to the measuring location. Therefore, under current measuring resolution (60 mm x 60 mm), the measurement in CS9 may fail to capture the large velocity of the jet. The experimental data in CS8 shows that the flow from the gaspers first merged with the flow from the diffusers and then flowed downward toward the aisle. Compared with the air distribution in CS8, the merged flow in CS9 was much weaker. The CFD simulation in this study used the measured flow from the diffusers as the boundary conditions. Since the velocity at the diffusers differed from row to row, the air distributions in CS8 and CS9 were different. Nevertheless, the general trend of the flow was mixing ventilation at the two cross sections. The upward flows above the passengers were due to the thermal plumes caused by the body heat. Similar results were observed in the CFD simulation results. However, the air velocity calculated by CFD differed significantly from the measured data on both sides of CS8. The CFD simulation assumed that the manikins had uniform temperature in each section of the head, upper body, and lower body. Since the two sides of CS8 were affected by the buoyancy from the heated manikins, the difference may have been caused by the discrepancy between the actual temperature profile and that used as the CFD boundary condition.

In the longitudinal sections, the experimental results showed that the air traveled from the front to the back of the cabin. This is because the measured velocity component in the longitudinal direction had a clear backward trend. Since the experimental data from the diffusers was used as the boundary conditions for the CFD simulation, the calculated air velocity also exhibits longitudinal transport toward the back of the cabin. Although the

agreement between the CFD prediction and the experimental measurements is not as good as that for the one-row cabin, the CFD simulation results are acceptable due to the many uncertainties associated with the measurements for such a complex scenario.

Figure 9 further compares the predicted and measured temperature fields in the CS9 and ASLS sections. Since the airflow in the cabin was well mixed, the temperature distribution should have been relatively uniform. The CFD simulation with the simplified gasper model was able to predict the uniform temperature field. At CS9, the air temperature in the center of the cabin was lower than the rest of the cabin, because the central region was in the path of cool air from the diffusers and gaspers. The air temperature on the upper right side of the cabin was higher than in the rest of the cabin. It should be noted that the flow boundary conditions of the diffusers were very complex (Liu et al., 2012b), and at times the flow direction could even be toward a diffuser. Therefore, the high temperature in that area may have been caused by air circulation that was due to the complexity of the flow in the region.

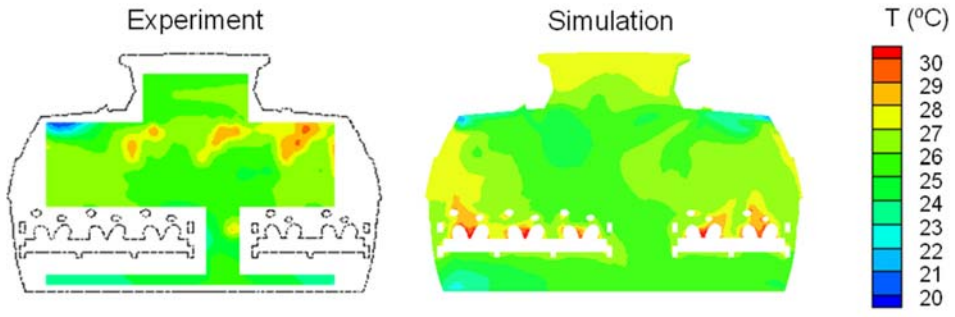

(a)

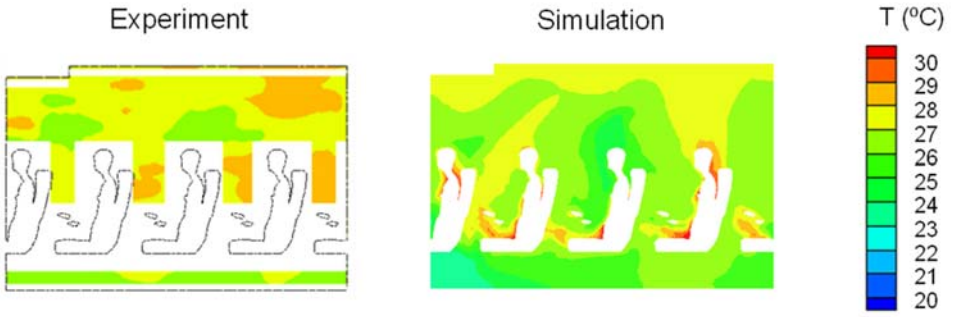

(b)

Figure 9 Comparison between the predicted and measured temperature field in (a) CS9, and (b) ASLS.

At section ASLS, the measured air temperature was about 1.0 K higher than the simulated temperature. The difference may have been caused by experimental error, as the two sections were not measured at the same time. The air temperature in the upper part of the cabin was

slightly higher than in the lower part. The same trend was observed in the air temperature distribution calculated by CFD. Because of the obstructions created by the seat backs and the complex airflow pattern, it is difficult to perform a quantitative comparison of the calculated and measured air temperature distributions. Note that the air temperature fields were measured with a precision of ±0.5 K (Li et al., 2016). As the difference between the predicted and measured data was less than 1.0 K, the CFD simulation results are considered to be good.

This study also compared the simulated and measured SF_6 concentration distributions at sections CS9 and ASLS because the SF_6 source was located in these two sections, as shown in Figure 10. Since the air was supplied symmetrically from the diffusers and gaspers, the flow at CS9 was almost symmetric. Thus, SF_6 from the source in seat 9C was contained on the left side of the cabin, as shown in both the measured and calculated results. The CFD results agree well with the measured data in this section.

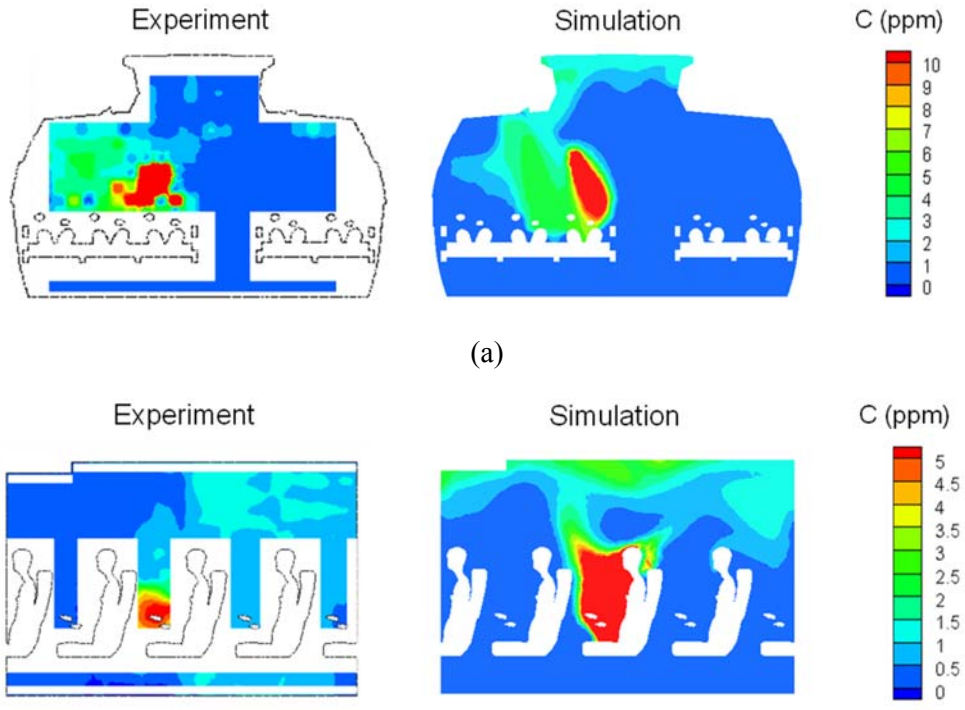

Figure 10 Comparison between predicted and measured contaminant concentration in (a) CS9, and (b) ASLS.

However, the measured SF_6 distribution at section ASLS shows that the SF_6 moved upward from seat 9C and travelled toward the back rows, but the backward trend was not captured very well by the simulation. As can be seen in the air velocity distribution in Figure 8(a), the predicted flow direction at the source location was downward, but the measured flow

direction was upward. This difference could be a major reason for the discrepancies in SF_6 dispersion.

4. Discussion

This study used the simplified gasper model in a CFD simulation of a five-row section of the economy-class cabin. If this method were applied to the entire 28-row economy-class cabin, the total grid number would be 21 million, and the computing time would be around one week on our small workstation, which is still feasible. However, if the detailed gasper geometry were applied to the whole cabin, the total grid number would be over 100 million. This would require a large computer cluster and significant computing time, which might not be feasible for design studies. The simplified gasper model can dramatically reduce the total grid number and computing time needed to predict contaminant transport in aircraft cabins without compromising accuracy. Thus, the method for simplifying the gasper geometry could be used in future investigations to study the aircraft cabin environment with gaspers on.

In addition to gaspers, diffusers with complicated geometry are commonly used in aircraft cabins and buildings. The advanced aircraft cabin in the Boeing 747-8 has about 50 slots per row on each side of the cabin shoulder and ceiling as diffuser outlets. The supply air from a duct is directed to the slots by an array of nozzles with extremely complicated geometry. In buildings, round and square diffusers are commonly installed. The round diffusers supply air through concentrically annular outlets, and the square diffusers through multiple slots. Using the detailed geometry for these diffusers could result in large grid numbers and high computing costs. The concept proposed in this study for simplifying the gasper geometry could also be used to simplify the complex geometry of the diffusers in aircraft and buildings.

5. Conclusions

This investigation proposed a method for simplifying the geometry of a gasper to a round nozzle. The simplified gasper model was implemented in CFD to replace the complex gasper geometry for predicting air distribution and contaminant transport in an aircraft cabin. The predicted results were validated by experimental data in two cases: a cabin mockup and a real cabin. Within the scope of this research, the following conclusions can be drawn:

(1) The proposed method for simplifying the gasper geometry as a round nozzle could ensure that the jet from the nozzle and the jet from the complex gasper geometry have the same downstream velocity field.

(2) Compared with the detailed gasper geometry in the CFD simulation for the cabin mockup, the simplified gasper model reduced the grid number from 1.58 million to 0.3 million and the computing time from 2 days to 1 hour without compromising accuracy.

(3) The CFD simulation with the simplified gasper model was acceptable in predicting the distributions of air velocity, air temperature, and contaminant concentration in a five-row section of the economy-class cabin of the MD82 airplane.

Acknowledgements

The research presented in this paper was supported by the National Basic Research Program of China (the 973 Program) through Grant No. 2012CB720100 and the Chinese Natural Science Foundation through Grant No. 51478302.

References

ACI (Airports Council International). 2007. "The Global Airport Community." www.airports.org/aci/aci/file/AnnualReport/ACIAnnualReport2006FINAL.pdf.

ANSYS. 2010. " Fluent 12.1 Documentation." Fluent Inc., Lebanon, NH.

Dai, S., H. Sun, W. Liu, Y. Guo, N. Jiang, and J. Liu. 2015. "Experimental study on characteristics of the jet flow from an aircraft gasper." Building and Environment 93: 278-284.

Gupta, J. K., C-H. Lin, and Q. Chen. 2012. "Risk assessment for airborne infectious diseases in aircraft cabins." Indoor Air 22: 388-395.

Hussein, H. J., S. P. Capp, and W. K. George. 1994. "Velocity measurements in a high-Reynolds-number, momentum-conserving, axisymmetric, turbulent jet." Journal of Fluid Mechanics 258: 31-75.

Kenyon, T. A., S. E. Valway, W. W. Ihle, I. M. Onorato, and K. G. Castro. 1996. "Transmission of multidrug resistant mycobacterium tuberculosis during a long airplane flight." New England Journal of Medicine 334: 933-938.

Li, B., J. Li, Y. Huang, H. Yin, C-H. Lin, D. Wei, X. Shen, J. Liu, and Q. Chen. 2016. "Experimental studies of thermal environment and contaminant transport in a commercial aircraft cabin with gaspers on." Indoor Air doi: 10.1111/ina.12265.

Liu, W., S. Mazumdar, Z. Zhang, S.B. Poussou, J. Liu, C-H. Lin, and Q. Chen. 2012a. "State-of-the-art methods for studying air distributions in commercial airliner cabins." Building and Environment 47: 5-12.

Liu, W., J. Wen, J. Chao, W. Yin, C. Shen, D. Lai, C-H. Lin, J. Liu, H. Sun, and Q. Chen. 2012b. "Accurate and high-resolution boundary conditions and flow fields in the first-class cabin of an MD-82 commercial airliner." Atmospheric Environment 56: 33-44.

Liu, W., J. Wen, C-H. Lin, J. Liu, Z. Long, and Q. Chen. 2013. "Evaluation of various categories of turbulence models for predicting air distribution in an airliner cabin." Building and Environment 65: 118-131.

Menter, F. R. 1994. "Two-equation eddy-viscosity turbulence models for engineering applications." AIAA Journal 32: 1598-1605.

Moser, M. R., T. R. Bender, H. S. Margolis, G. R. Noble, A. P. Kendal, and D. G. Ritter. 1979. “An outbreak of influenza aboard a commercial airliner.” American Journal of Epidemiology 110: 1–6.

Olsen, S. J., H. Chang, T. Y. Cheung, A. F. Tang, T. L. Fisk, S. P. Ooi, H. Kuo, D. D. Jiang, K. Chen, J. Lando, K. Hsu, T. Chen, and S. F. Dowell. 2003. “Transmission of the severe acute respiratory syndrome on aircraft.” The New England Journal of Medicine 349: 2416-2422.

Patankar, S. V. 1980. Numerical Heat Transfer and Fluid Flow. New York: Hemisphere Publishing Corp.

Pope, S. B. 2000. Turbulent Flows. Cambridge: Cambridge University Press.

Shi, Z, S. Dai, J. Chen, and Q. Chen. 2015a. "Numerical study of gasper-induced jet flow withdetailed gasper geometry," Proceedings of the 9th International Symposium on Heating, Ventilating and Air-Conditioning (ISHVAC) and the 3rd International Conference on Building Energy and Environment (COBEE), Tianjin, China. Paper No. T6-573, 9 pages.

You, R., J. Chen, Z. Shi, W. Liu, C-H. Lin, D. Wei, and Q. Chen. 2016.” Experimental and Numerical Study of Airflow Distribution in an Aircraft Cabin Mockup with a Gasper On.” Journal of Building Performance Simulation doi:10.1080/19401493.2015.1126762.

Zhang, Z., and Q. Chen. 2007. "Comparison of the Eulerian and Lagrangian methods for predicting particle transport in enclosed spaces," Atmospheric Environment 41(25): 5236-5248.

Zhang, Z, X. Chen, S. Mazumdar, T. Zhang, and Q. Chen. 2009. “Experimental and numerical investigation of airflow and contaminant transport in an airliner cabin mockup.” Building and Environment 44: 85-94.